Pulsed laser deposition of thin superconducting films of $Ho_1Ba_2Cu_3O_{7-x}$ and $Y_1Ba_2Cu_3O_{7-x}$

D. B. Geohegan, D. N. Mashburn, R. J. Culbertson, S. J. Pennycook, J. D. Budai, R. E. Valiga, B. C. Sales, D. H. Lowndes, L. A. Boatner, E. Sonder, D. Eres, D. K. Christen, and W. H. Christie
Solid State Division, Oak Ridge National Laboratory, Oak Ridge, Tennessee 37831-6056

(Received 1 June 1988; accepted 9 August 1988)

Thin films of $Ho_1Ba_2Cu_3O_{7-x}$ and $Y_1Ba_2Cu_3O_{7-x}$ were deposited on $SrTiO_3$ and Al_2O_3 substrates by pulsed laser deposition of high-T_c bulk superconductor pellets in vacuum. Following annealing in O_2 at 800–900 °C the films were superconducting with typical T_c (50%) = 89 K and transition widths of 10 K. Rutherford backscattering spectrometry (RBS) and secondary ion mass spectrometry (SIMS) were utilized to study the stoichiometry of the as-deposited films for laser energy densities between 0.11 and 4.5 J cm^{-2}. The films were deficient in holmium and yttrium for energy densities below 0.6 and 0.4 J cm^{-2}, respectively. The films were stoichiometric for fluences above 0.6 J cm^{-2}. In addition, preliminary time dependence and spectroscopic observations of the laser-produced plasma are presented. The results indicate an ablation mechanism that at high energy densities preserves stoichiometry. TEM and x-ray characterization of annealed, superconducting $Ho_1Ba_2Cu_3O_{7-x}$ films on (100) $SrTiO_3$ showed mixed regions of epitaxially oriented 1:2:3 material with either the *c* axis or *a* axis oriented along the surface normal. The *a*-axis-oriented material grew preferentially in the films with *b*, *c*, twinning.

I. INTRODUCTION

Since the first characterizations of the interaction of high-powered laser radiation with solid surfaces over 20 years ago,[1,2] the technique of pulsed laser vaporization has been used to deposit a wide range of materials including metals,[3] semiconductors,[4–10] and dielectrics.[3,5,7,8,11,12] The technique has been limited, however, by problems associated with the complex vaporization process such as incongruent stoichiometry transfer between target and film, particulate formation[2,9,10] ("spitting"), ion damage of films by the laser-induced plasma[13] and, underlying these, lack of a physical understanding of the laser ablation process. These problems have been overcome experimentally in many cases and, by careful control of the laser power and wavelength, epitaxial semiconductor films[9,10,14] and superlattices have been grown.[15,16]

Recently, the pulsed laser deposition technique has been applied successfully to deposit thin films of the high-T_c oxide superconductors $Y_1Ba_2Cu_3O_{7-x}$[17–22] and $La_{1.85}Sr_{0.15}CuO_{4-x}$.[21] The attractiveness of this technique is that the 1:2:3 stoichiometry of the target material (usually a bulk superconducting pellet) can be reproduced relatively easily in the films, to within about 10%. At low laser energy densities, however, deficiencies of yttrium have been reported in annealed films.[18,23]

In this paper we describe pulsed laser deposition of thin superconducting films of $Ho_1Ba_2Cu_3O_{7-x}$ and $Y_1Ba_2Cu_3O_{7-x}$ on a variety of substrates ($SrTiO_3$, Al_2O_3, and SiO_2 on Si). In a previous paper, we reported a lack of stoichiometry in oxygen-annealed thin films formed by pulsed laser ablation of $Y_1Ba_2Cu_3O_{7-x}$ at low fluences.[18] Here the stoichiometry of as-deposited films of $Ho_xBa_yCu_zO_\delta$ and $Y_xBa_yCu_zO_\delta$ was characterized as a function of the actual laser energy density delivered to the pellet, in order to investigate the mechanism of the ablation process and to determine a range of useful deposition conditions. Scanning-electron micrographs of the as-deposited films, as well as preliminary measurements of the emission spectra and time-dependent intensity of the laser-induced plume also are presented as an aid to understanding the pulsed laser deposition process. The superconducting properties and microstructure of the annealed $Ho_1Ba_2Cu_3O_{7-x}$ superconducting films, as revealed by transmission electron microscopy (TEM) and x-ray diffraction (XRD), are also presented.

II. EXPERIMENTAL

The deposition process utilizes a high-power, pulsed excimer laser to ablate material from the face of a superconducting pellet onto a nearby substrate. A schematic of the experimental apparatus has been published elsewhere.[18] The pellet (target) was mounted in a copper ring and positioned by a vertical support rod 2–3 cm away from a heated substrate under vacuum (1×10^{-6} Torr). The pellet was irradiated by pulsed 248 nm (25 ns FWHM) light from a KrF laser (Questek 2640). An external cylindrical lens focused the rectangular excimer beam to a line on the pellet (typically 1.2×0.015 cm), producing peak intensities of up to 280 MW cm^{-2}.

 0884-2914/88/061169-11$01.75

The high local electromagnetic fields produced a white plasma at the surface of the pellet and a visible plume of excited vapor extending toward the substrate.[24]

The substrates were held in contact with the 1 in. square ceramic face of a resistive heater by a copper mask under spring tension. A thermocouple was firmly fastened to the heater by a metal clip. This heater assembly was supported by a quartz rod that could be rotated or translated without breaking vacuum due to an O-ring seal.

The Pyrex vacuum chamber has multiple ports for sample, target, laser beam, and diagnostic access. The chamber was pumped with a turbomolecular pump and was connected to a gas manifold to permit the introduction of high-purity oxygen or helium. Quartz (Suprasil 1) entry and exit windows were used for the excimer laser beam. An energy meter (Scientech 365) was mounted behind the exit window of the chamber and was used both to initially calculate and to periodically monitor the energy delivered through the front window. A low-power cw He–Ne laser beam passing through the entrance window of the chamber was used to detect any decline of transmitted laser power due to film deposition on the window during a run.

In order to define the area of the focused laser beam at the target, the intensity profile across the narrow (vertical) beam dimension was measured at the working distance used during the depositions. With the laser average power held constant by microprocessor control, an attenuated beam was focused onto a 20-μm slit that was aligned parallel to the line focus and scanned across it. The transmitted energy passing through the slit was measured with a Scientech 365 power meter. The measured beam profile at the focus was closely approximated by a Gaussian curve with a full width at half-maximum (FWHM) of 150 μm. This FWHM contained 76% of the energy in the beam. Accordingly, the fluences quoted in this paper were calculated using 76% of the pulse energy delivered to the target divided by the effective beam area (i.e., length times FWHM).

Film thicknesses ranged from 0.1 to 3 microns with deposition rates from <1 to 10 Å per pulse. The substrate temperature was typically maintained at 400 °C to allow surface mobility of the deposited species while limiting oxygen out-diffusion. The as-deposited films discolored rapidly (in minutes) upon exposure to room air. However, an *in situ* treatment in oxygen at 400 °C (1–100 mTorr, 15 min) stabilized the films against the atmosphere and gave them a smooth, dark, and shiny appearance.

All films have required conventional annealing in an oxygen furnace (800–900 °C) to become metallic and superconducting. A range of annealing conditions were investigated and correlated with resistance measurements made with a four-point probe. Two anneals were employed. A slow anneal involved heating the stabilized films at 3 C°/min to 880 °C in 1 atm O_2 where they were held for 1 h. The films were then cooled to 450 °C at 15 C°/min where they were held for 12–14 h and then brought to room temperature at 5 C°/min. A fast anneal involved inserting the films quickly into the 900 °C hot zone of the furnace instead of the slow ramp up to temperature, followed by cooling to 450 °C at 20 C°/min where they were held for 6 h and then brought to room temperature at 5 C°/min. The implications for the formation of the superconducting orthorhombic phase and the effect on surface morphology will be discussed in the next section.

III. RESULTS AND DISCUSSION

A. Characterization of the pulsed laser deposition process—Stoichiometry of as-deposited films

Figure 1 shows a representative SEM micrograph of an as-deposited $Ho_xBa_yCu_zO_\delta$ film on SiO_2; the film was overcoated with 200 Å of gold to reduce surface charging. The films were generally smooth with $\leqslant 1$ μm particles impacted into the surface in densities that increased with laser energy density. The particles were observed at all energy densities studied. At the lowest energy densities, the particles stood elevated from a very smooth film that appeared to be formed by condensed, transported vapor. At the highest energy densities, the particles showed evidence of having been molten upon impact. The two components of the film morphology have been noted in almost every study of pulsed-laser evaporated films and the particle density has been reported to be reduced by lowering the laser intensity or rotating the target. Particulate formation ("spitting" of molten particles from the pellet) is believed to be caused by the expulsion of superheated subsurface melted target material when some of the material vaporizes.[2]

A principal challenge of the pulsed laser deposition process is to achieve the desired stoichiometry in the deposited film. When heated by pulsed laser irradiation, multicomponent targets sometimes evaporate noncongruently due to the variation in the melting points and vapor pressures of the constituents. At low-energy densities, differences between the stoichiometry of the deposited films and the $Y_1Ba_2Cu_3O_7$ and $Ho_1Ba_2Cu_3O_7$ targets were observed.

Figure 2 shows the results of RBS measurements on two films deposited from the same $Y_1Ba_2Cu_3O_7$ pellet using focused energy densities of (a) 0.2 J cm^{-2} and (b) 2.1 J cm^{-2}. The annealing procedure described earlier was used for both films. In order to compare the relative stoichiometry of the films, the Ba concentration was normalized to 2.0 for each sample. Instead of the expected $Y_1Ba_2Cu_3O_7$ stoichiometry, the film deposited using

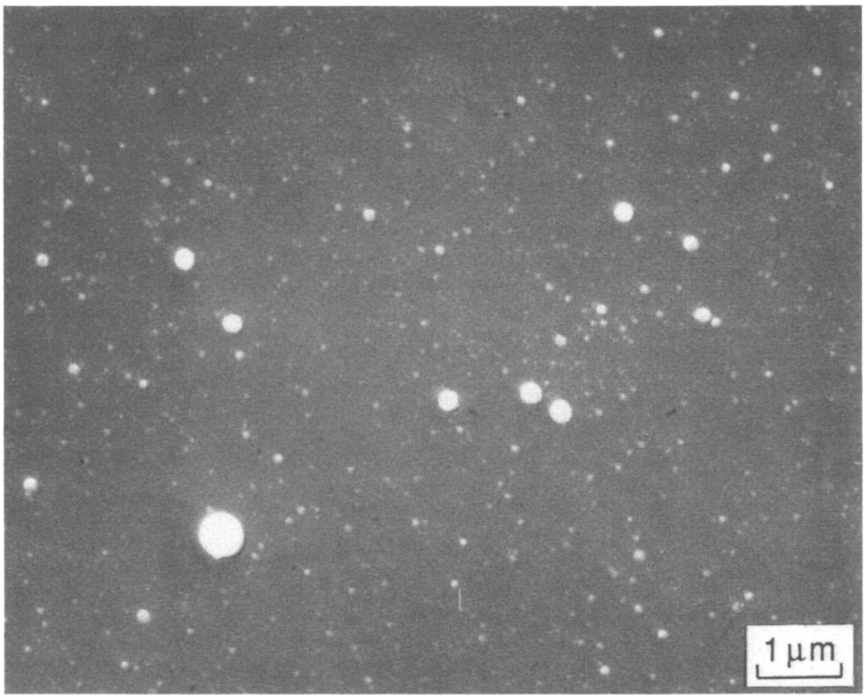

FIG. 1. SEM micrograph of the surface of an as-deposited 5000 Å thick film of $Ho_xBa_yCu_zO_\delta$ formed by irradiation of a $Ho_1Ba_2Cu_3O_7$ pellet with 1.2 J cm^{-2} (248 nm) laser pulses for 100 s at 20 Hz. Ejected, spherical particles from the target appear white on the grey background of the smooth film formed by condensed vapor from the plume. The film was overcoated with 200 Å of gold to prevent surface charging.

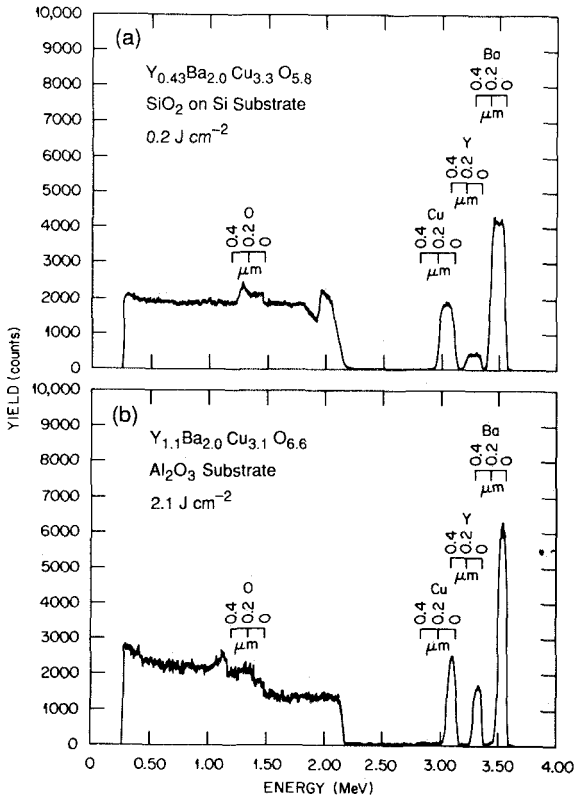

FIG. 2. RBS spectra of thin films made by ablating bulk $Y_1Ba_2Cu_3O_7$ with different focused laser energy densities of (a) 0.2 J cm^{-2} and (b) 2.1 J cm^{-2}. The 0.2 J cm^{-2} film is yttrium deficient. The stoichiometries were normalized to Ba = 2.0. Shown above the different peaks are distance markers which indicate the penetration depths of the components (where 0 represents the film surface) into the film.

an energy density of 0.2 J cm^{-2} was yttrium deficient [as in Fig. 2(a): $Y_{0.43}Ba_{2.0}Cu_{3.3}O_{5.8}$) and was semiconducting after oxygen annealing. Raising the laser energy density at the target to 2.1 J cm-2 corrected the yttrium deficiency [as in Fig. 2(b): $Y_{1.1}Ba_{2.0}Cu_{3.1}O_{6.6}$] and yielded films of stoichiometry within 10% of the target. These observations ($< 10\%$ estimated error) were corroborated by energy dispersive x-ray (EDX) measurements.

Qualitative observations of the plume in the high- and low-intensity regimes suggested an explanation for the change in stoichiometry. At low intensities, a plume would form immediately, losing intensity to a constant, very weak fluorescence within 40 laser shots. (Similar first-strike effects have been noted in laser irradiation of semiconductors and were attributed to the vaporization of surface contaminants.[25]) After repeated shots, the irradiated region of the pellet appeared shiny and metallic. At high fluences, however, the focused radiation cut deep grooves into the pellet and produced an intense white plasma at the surface for each shot.

The stoichiometry and morphology of the pellet also were examined for the high and low intensity regimes. Scanning electron micrographs of a sintered and annealed $Y_1Ba_2Cu_3O_7$ pellet are shown in Fig. 3. The unirradiated surface of the pellet in Fig 3(a) was composed of < 1 μm diam microcrystallites. The region irradiated at 0.2 J cm^{-2} [Fig. 3(b)] appears to have undergone surface melting, producing resolidified ≈ 10 μm features. (Similar conical features have been observed following XeCl laser polyimide ablation[26]; these

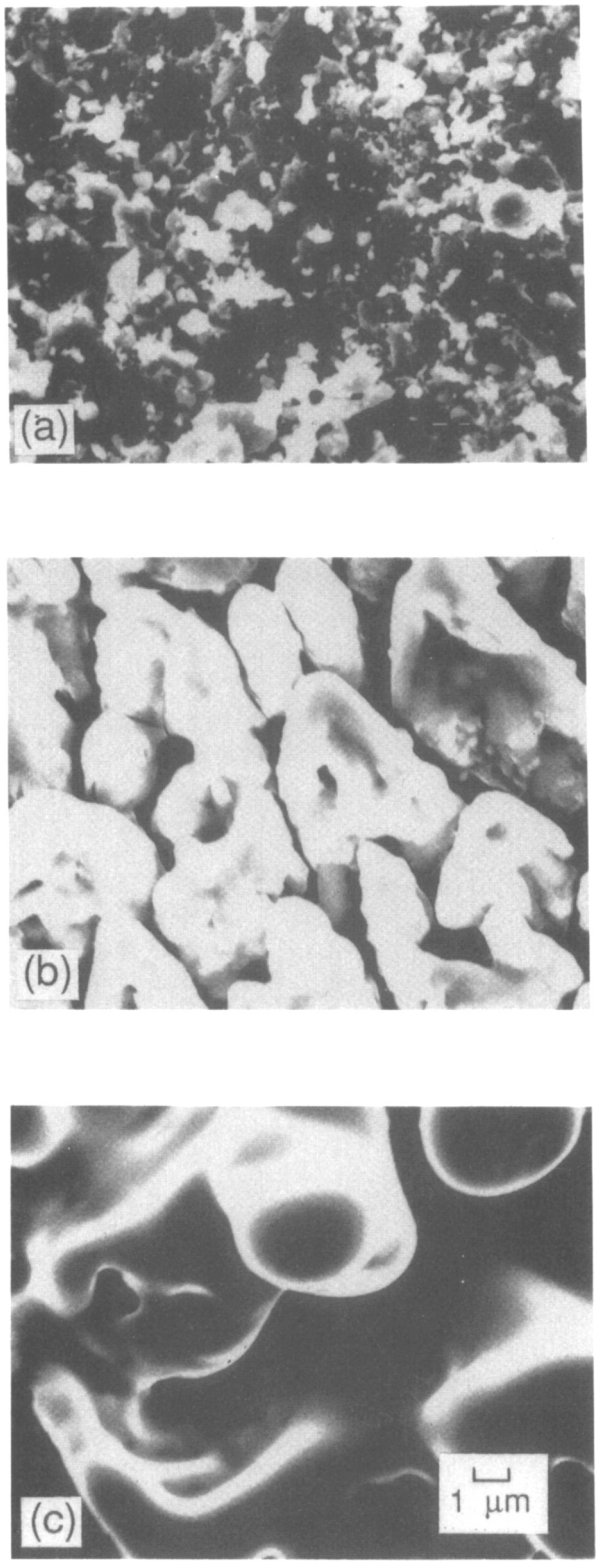

FIG. 3. SEM micrographs of the surface of a bulk superconducting $Y_1Ba_2Cu_3O_7$ pellet (a) before and (b), (c) after pulsed laser irradiation at 248 nm. Region (b) received 2000 laser pulses at 0.2 J cm^{-2} and was yttrium rich. Region (c) received 1000 laser pulses at 2.1 J cm^{-2} and was of the 1:2:3 stoichiometry of the pellet. Region (c) was accompanied by a bright white plasma at the surface during irradiation.

were attributed to shielding effects from $\sim\mu$m-sized particles on the target surface in the near-threshold ablation regime. Also, Auciello, *et al.*[27] have also recently reported conical features dominating XeCl laser-irradiated $Y_1Ba_2Cu_3O_7$ pellets after ~ 1200 laser shots.)

EDX measurements confirmed that this region was yttrium-rich, indicating that the surface temperature increase was insufficient to evaporate much yttrium, resulting in the yttrium-deficient film of Fig. 2(a). At higher intensities, however, where the plasma was formed at the surface [such as the region irradiated at 2.1 J cm^{-2} shown in Fig. 3(c)], smoothed large pits suggest a much more efficient melting of the pellet. EDX measurements of the 2.1 J cm^{-2} region showed the same stoichiometry as the unirradiated region of the pellet.

The annealed $Ho_xBa_yCu_zO_\delta$ films displayed the same rare-earth-element transport behavior. At low energy densities the annealed films were deficient in Ho and stoichiometric in Ba and Cu. Various annealing conditions were attempted with the nonstoichiometric films but they remained semiconducting, as expected. In order to define the range of energy densities over which stoichiometric films could be obtained, a series of "as-deposited" films were made and examined for stoichiometry following oxygen stabilization but without annealing at high temperature. Sets of 8–10 films were deposited within minutes of each other while the KrF laser beam energy was attenuated with quartz flats. The pellet-to-substrate separation was fixed at 2.5 cm and the temperature was held constant at 400 °C. A 5×5 mm aperture cut in a Be–Cu mask was positioned 1.5 cm away from the pellet to define a deposition region on the substrate that was along the normal line from the irradiated surface. The heater then was rotated and translated (without changing the spacing) to reveal fresh regions of the substrate. Hence, the same position in the plume (normal to the irradiated region of the pellet) was maintained for each deposition. A fresh region of the pellet was used for each deposition but neither the pellet's separation from the substrate nor the beam focus was changed. These "as-deposited" films were stabilized against exposure to the atmosphere by an *in situ* treatment in 1 Torr O_2 at 450 °C for 15 min and then cooled to room temperature at 20 C°/min. RBS and SIMS were then employed to determine the stoichiometry of the films.

RBS analyses of the series of "as-deposited" $Ho_xBa_yCu_zO_\delta$ films on Al_2O_3 used 5 MeV He^+ ions. EDX measurements of the films indicated that the Ba concentration remained closest to that of the pellet in depositions at various energy densities. Hence, the stoichiometry ratio x:y:z for these films is displayed in Fig. 4 by normalizing the Ba concentrations to $y = 2.0$. Error bars on the points include statistical errors (typical-

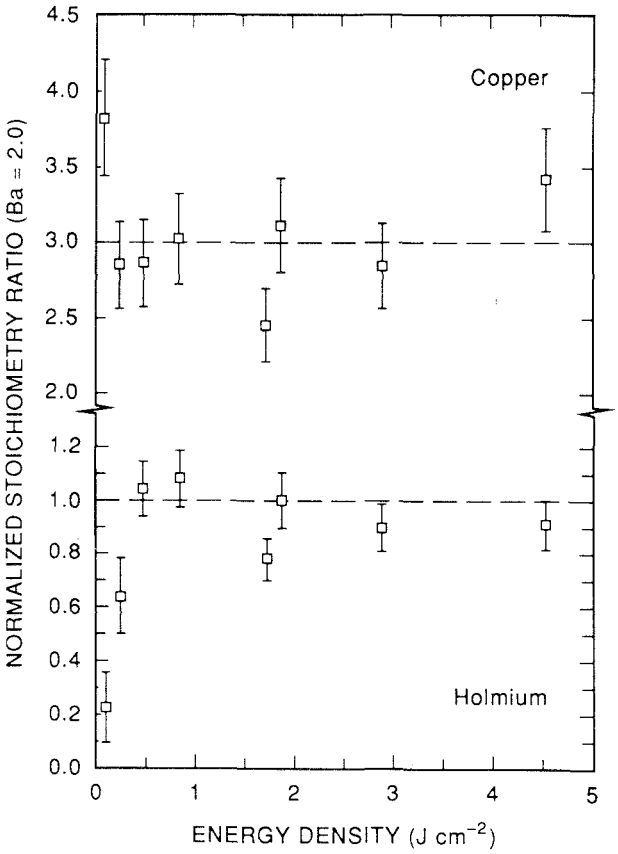

FIG. 4. RBS stoichiometry survey of "as-deposited" $Ho_xBa_yCu_zO_\delta$ films made by pulsed laser evaporation of bulk $Ho_1Ba_2Cu_3O_7$ at energy densities from 0.11 to 4.4 J cm^{-2}. For comparison, the barium concentration was normalized to $y = 2.0$.

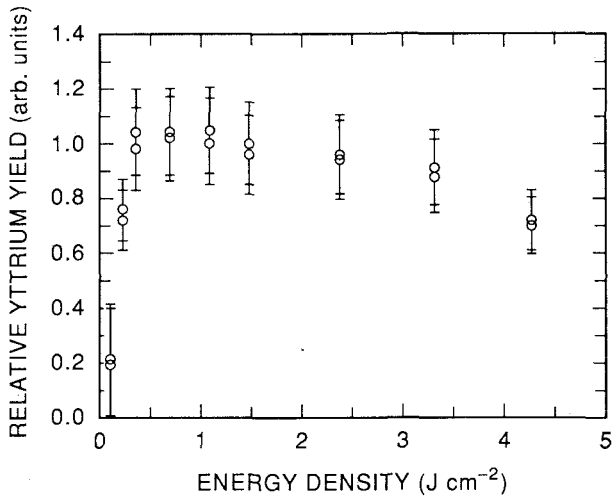

FIG. 5. Yttrium content of $Y_xBa_yCu_zO_\delta$ "as deposited" films versus laser energy density incident on the pellet as determined by SIMS absolute-yields depth profiles. Two measurements were made for each film.

ly 3%–7%) and possible errors due to overlap of the Ho and Ba backscattering peaks. With the exception of the point at 1.7 J cm^{-2} (possibly a Ba-rich film), the stoichiometry of the films for energy densities $\geqslant$0.6 J cm^{-2} can be viewed as constant, displaying the same 1:2:3 stoichiometry as the pellet (indicated by the dashed lines in Fig. 4). Below 0.6 J cm^{-2} the films' Ho concentration was deficient with respect to the pellet, while the Cu concentration was enriched at the lowest fluence.

In order to independently confirm the difficulty with rare-earth-element transport at low-energy densities, a series of "as-deposited" $Y_xBa_yCu_zO_\delta$ films were examined by SIMS for absolute yttrium yield versus depth. Nine films were deposited on Au-overcoated SiO_2 in vacuum at 450 °C and oxygen-stabilized. The SIMS depth profiles were extremely flat, displaying occasional deviations from the average that indicated yttrium-rich planes at certain depths. Figure 5 gives the averaged yttrium yield for each of the films (two profiled spots per film) with error bars including the maximum observed deviation from average and the possible errors due to differences in ion-collection efficiency between samples. Like the Ho data, the Y concentration displayed two regimes: films deposited with energy densities below 0.4 J cm^{-2} were yttrium-deficient while energy densities above 0.4 J cm^{-2} resulted in films of nearly constant yttrium concentration.

No evaporation from either $Y_1Ba_2Cu_3O_7$ or $Ho_1Ba_2Cu_3O_7$ pellets could be achieved for energy densities $<$0.11 J cm^{-2}. This agrees with recent measurements by Inam *et al.*[28] in which the threshold energy density for pulsed laser etching of Y–Ba–Cu–O films in air was determined to be 0.11 J cm^{-2}.

The two intensity regimes noted in the stoichiometry studies coincide closely with the onset of the laser-induced plasma that is formed at the pellet surface at the higher laser intensities. In the low-intensity regime (energy densities $<$0.6 J cm^{-2}) the plume is faint orange without the bright white plasma along the surface. In this regime, the stoichiometry of the as-deposited films and the morphology and stoichiometry of the pellet indicate that deposition is primarily due to laser evaporation of the surface. The temperature at the pellet may have been sufficient to melt the compound but the evaporation rates of the different constituents appear to have followed the vapor pressures of the metals or their oxides. The vapor pressures of the constituent elements at elevated temperatures (e.g., 0.0016, 150, and 0.43 Torr for Y, Ba, and Cu, respectively, at 1500 °C), suggest that Y would be more difficult to evaporate from a mixture of the elements under near-thermal equilibrium pulsed laser heating. The same Y transport difficulty should also be expected based upon evaporation of targets composed of the oxides Y_2O_3, BaO and CuO. The vapor pressures (and vaporization rates) of the oxides[29] show that Y_2O_3 (and Ho_2O_3) require much higher temperatures to vaporize than BaO or CuO. CuO liberates oxy-

gen readily in vacuum at elevated temperatures (and hence the vapor pressure follows that of Cu metal) while BaO and Y_2O_3 preferentially vaporize as oxides yielding predominantly BaO (with 10^2 to 10^3 times less Ba vapor from 1500 to 3000 K) and YO (with O, Y_2O, and Y_2O_2 as secondary byproducts), respectively. The relative vapor pressures of BaO and Y_2O_3 at 1500 °C, for example, are 4.9 mTorr and 2.0×10^{-9} Torr, respectively. Recent experiments involving strict evaporation of multioxide targets by cw CO_2 laser evaporation found similar yttrium deficiencies (and stoichiometric Ba and Cu) in deposited films.[30] This was compensated by enriching the yttrium concentration in the target by a factor of ~4.

At high intensities, where a strong plasma has formed, the interaction with the surface is an indirect process which, in this case, preserves stoichiometry. This explanation is based upon the large amount of work that has been performed on laser vaporization of metals, semiconductors and compressed powders in which vaporization processes have been related to similar energy density regimes.[31-33] For metal targets with $<10^8$ W cm^{-2} incident laser intensities, for example, the laser vaporizes material due a direct heating of the surface. At higher laser intensities, however, the vaporization process becomes indirect due to the formation of a plasma near the surface of the target.[2] A plasma forms when the evaporated vapor above the surface absorbs the laser energy in the presence of seed electrons. The plasma can easily form within a 50 ns laser pulse and shows up as a "flash" or plume of fluorescence due to recombination and deexcitation of excited states of the vaporized material within the plasma. Depending on the duration of the pulse and the density of ejected vapor, the plasma can then effectively screen the target[31] from the remainder of the laser pulse, absorbing the laser photons by inverse Bremmstrahlung, thereby heating the plasma and causing an expansion of the plume away from the surface at velocities as high as 10^6–10^7 cm s^{-1}. For pulses in the microsecond to millisecond time scale, the plasma can subsequently reinitiate,[2,32] persisting in a steady state throughout the laser pulse, fed by the removal of material from the target. In this case, material removal is controlled by a plasma interaction with the substrate, indirectly fueled by the laser energy. The nature of the interaction is presumably radiative heating of the surface by the localized plasma.

However, preliminary measurements of the time dependence of the plume fluorescence in the high-intensity regime of these experiments indicated that emission from the bright plasma nearest the substrate reaches its maximum within the duration of the laser pulse. The side-looking fluorescence of the bright plasma formed at the pellet surface was collected with a lens and focused onto a Hamamatsu R1193U-07 vacuum photodiode. The time dependence was displayed on a Tektronix 7104 oscilloscope. The extremely bright fluorescence at the pellet surface initiated ~7 ns after the arrival of the laser pulse. This rapid signal peaked 24 ns later, subsequently decaying exponentially ($\tau=60$ ns time constant). The remainder of the fluorescence (from the entire spatial region between the target and substrate) reached a maximum following the laser pulse and decayed with a 150 ns time constant, lasting nearly 1 μs. From the above observations, one can conclude that the plasma observed at the pellet surface does not reinitiate over the time scale of the laser pulse. The production of radiative species close to the surface appears to end within the duration of the laser pulse. The observation of fluorescence far from the pellet at later times indicates either an expansion of the plume away from the pellet with different velocities or additional processes for producing radiating species in the gas phase, due to electron collisions in the cooling, expanding plasma.

Hanabusa *et al.*[4] have observed very similar time dependences of Si* ($4s\ ^1P_1\rightarrow3p^2\ ^1D_2$) emission at the surface and 5 mm away from the surface following Nd:YAG laser (532 nm) vaporization of silicon. The time dependence of the emission far from the surface was described as resulting from the velocity distribution of the ejected particles that comprise the expanding vapor cloud (calculated to peak at a most probable velocity of $8\text{x}10^5$ cm s^{-1}). The actual temporal and spatial dependence of the plume fluorescence intensity, however, depends not only on the velocity distribution of the ejected particles but on the complex kinetics which govern the short-lived (<10 ns radiative lifetime) species observed nearly 1 μs after the laser pulse.

The brightest part of the plume is known to be a highly ionized plasma. As the plasma cools and expands, attachment and recombination processes become important and account for the change in emission observed in the plume at longer times and further distances from the pellet. A spectral survey of the plume was made over the 250–700 nm wavelength region in order to determine the emitting species. In addition to emission lines from monovalent Ba*, Cu*, Ba^+, and Cu^+, the emission spectrum contained overlapping vibrational bands from BaO ($A\ ^1\Sigma\rightarrow X\ ^1\Pi$) and CuO ($A\ ^2\Sigma\rightarrow X\ ^2\Pi$) in the orange, forming a continuum as viewed with the 10 Å resolution of a 0.25 m spectrograph/multichannel analyzer.

Addition of a background O_2 pressure significantly enhanced the plume intensity, with the increase dominated by BaO* and CuO* fluorescence. A spatial and temporal profile of the plume fluorescence as well as measurements of ion currents will be the subject of a later paper.

Theoretical[34] and experimental[35] characterizations of the angular distributions of material ejected in pulsed

laser vaporization are now being applied to the oxide superconductor materials. Recent measurements by Venkatesan *et al.*[36] of the angular distribution of the thickness and stoichiometry of KrF laser-deposited films from a $Y_1Ba_2Cu_3O_7$ pellet also reveal two distinct components in the vaporization process: (1) a nonstoichiometric ($\cos\theta$) evaporative component and (2) a highly forward-directed ($>[\cos\theta]^{11}$) component resulting from a second (as yet undetermined) ejection process. Although their stoichiometry ratios could not be used to determine the relative yttrium concentration from film to film (for a direct comparison with Fig. 5), their experiments qualitatively agree with our results: (1) At low-energy densities the pellet's vaporization is dominated by evaporation, producing nonstoichiometric films, and (2) the second ejection process preserves stoichiometry at the higher energy densities.

B. Microstructure and superconductivity of annealed $Ho_1Ba_2Cu_3O_{7-x}$ films

Figure 6 shows a representative resistance curve for a 1 μm film of $Ho_1Ba_2Cu_3O_{7-x}$ deposited on (100) $SrTiO_3$. The resistance profile of the bulk superconducting $Ho_1Ba_2Cu_3O_7$ pellet used in the depositions (T_c = 93 K) also is shown for comparison. While the onset superconducting transition temperatures of the films were nearly equal to those of the bulk materials, the widths of the transitions were broadened to 10 K (versus ~2 K). The origin of the broadened transitions was investigated by x-ray and TEM analyses.

Both as-deposited and annealed $Ho_1Ba_2Cu_3O_{7-x}$ samples grown on (100) surfaces of $SrTiO_3$ were examined by x-ray diffraction, using a four-circle diffractometer and Cu $K\alpha$ radiation. The as-deposited films showed broad scattering features characteristic of an amorphous structure with no evidence of crystalline peaks. Scans of a bare $SrTiO_3$ crystal showed that (100) crystal axis was tilted on the order of 1° from the normal to the surface, resulting in a surface lattice spacing of 3.90 Å.

X-ray scans of the annealed $Ho_1Ba_2Cu_3O_{7-x}$ samples showed that the films consist almost entirely of highly epitaxial 1:2:3 phase material which is oriented with either the a or c axis normal to the (100) $SrTiO_3$ surface (denoted $a\perp$ or $c\perp$, respectively). A θ-2θ scan along the surface normal (as shown in Fig. 7) revealed strong $a\perp$ diffraction peaks at the expected (h 00) Bragg angles with much smaller $c\perp$ (00l) components. The ratio of peak heights suggests approximately ten times more $a\perp$ material than $c\perp$. The alignment of both components was examined by ω scans of the (200) and (005) peaks, respectively. Both the a axis and the c axis were found to be aligned within 0.4°–0.9° (FWHM's of several ω scans) of the surface normal with a typical scan inset in Fig. 7. The positions of the peaks yielded lattice constants of $a = 3.84 \pm 0.005$ Å and $c = 11.65 \pm 0.01$ Å.

A search also was also made for $b\perp$ material. Due to the near coincidence of b with the $SrTiO_3$ lattice constant, scattering of material with the $b\perp$ orientation would be obscured by the strong $SrTiO_3$ substrate peaks in the near normal θ-2θ scan such as the one shown in

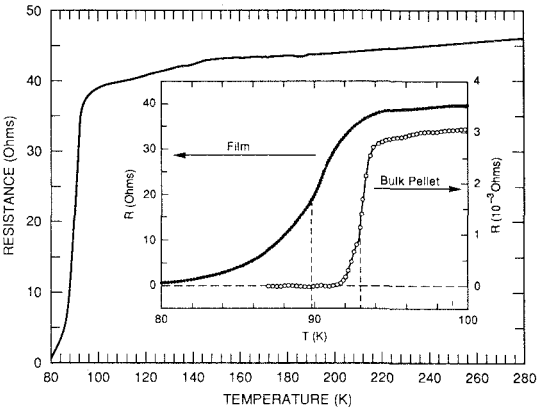

FIG. 6. Four-point probe resistance versus temperature profile of a 1 μm thick film of $Ho_1Ba_2Cu_3O_7$ deposited on $SrTiO_3$ in vacuum at 400 °C. The laser energy density used was 2.1 J cm^{-2}. The as-deposited film was slow-annealed in 1 atm O_2 at 900 °C for 1 h and cooled to 450 °C at 15 C°/min where it was held for 12–14 h and then brought to room temperature at 5 C°/min. The dashed lines indicate the 50% T_c values of 93 and 89 K for the bulk pellet and thin film, respectively.

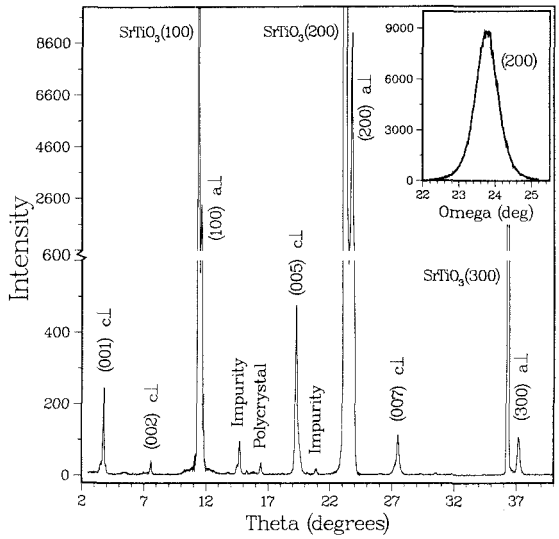

FIG. 7. An x-ray diffraction θ-2θ scan along the surface normal of an annealed $Ho_1Ba_2Cu_3O_{7-x}$ superconducting film on $SrTiO_3$. The film showed two phases of orthorhombic 1:2:3 material oriented with either the a or c axes normal to the (100) $SrTiO_3$ surface. A rocking curve of the strong (200) peak indicates epitaxial alignment with the $SrTiO_3$ to within 0.6°. The $a\perp$ material dominates the sample with a small amount of polycrystalline material indicated by the weak (013) and (103) powder lines. At least two peaks could not be assigned to the 1:2:3 material or the $SrTiO_3$.

Fig. 7. However, the presence of $b\perp$ material would also give rise to x-ray peaks at other predictable locations in reciprocal space which do not lie near cubic $SrTiO_3$ reflections. For example, the region of reciprocal space containing the orthorhombic (201) peak for $a\perp$ material would also contain a nearby (021) peak if $b\perp$ material were present. X-ray scans in two different regions [considering (201) vs (021) and (302) vs (032)] showed only well-defined single peaks in both the θ and 2θ directions at the positions expected for the $a\perp$ orthorhombic phase. The $b\perp$ component either was not present or was at most a few percent of the $a\perp$ component. These observations lead to two conclusions. First, we note that the $a\perp$ material has grown with an in-plane epitaxy such that the b and c axes lie along the cubic $SrTiO_3$ axes. Second, assuming comparable structure factors, we conclude either that the ratio of $b\perp$ to $a\perp$ material is very small or that the material has $a = b$ (tetragonal structure). The latter possibility can be eliminated on the basis of the superconductivity exhibited by the films.

Two of the strongest predicted powder lines [(103) and (013)] were barely discernible in the θ-2θ scan along the surface normal. Flat ω scans of these peaks indicated that the 1:2:3 films contained a small amount of randomly oriented polycrystalline material. In addition, weak reflections corresponding to d spacings of 3.03 Å, 2.16 Å, and 1.52 Å were detected in scans along the surface normal. Since these reflections exhibited sharp peaks in transverse ω scans, they are associated with an epitaxial impurity phase (or phases) and are possibly due to an interaction of the $SrTiO_3$ substrate with the films during annealing.

Cross sections of both the as-deposited and annealed $Ho_1Ba_2Cu_3O_{7-x}$ superconductor thin films were examined on a 100 keV transmission electron microscope . The as-deposited films were totally amorphous, in agreement with the x-ray measurements. A cross section of an annealed 0.3 μm $Ho_1Ba_2Cu_3O_{7-x}$ film on a $SrTiO_3$ substrate is shown in Fig. 8. In the low magnification view of Fig. 8(a), both the rough top-surface morphology and occasional cracks, which were also observed in the SEM, are seen. The crack extends into the $SrTiO_3$ substrate. A high-magnification view of the far left side of Fig. 8(a) is given in Fig. 8(b), showing the characteristic 11.7 Å lattice fringes. The two distinct epitaxial orientations noted by x-ray diffraction are clearly evident. Close to the substrate, the material was generally found to be oriented $c\perp$, with the majority of the material above it $a\perp$. The epitaxial alignment was maintained, despite the 90° rotation. The near-match between b and $c/3$ of the $Ho_1Ba_2Cu_3O_{7-x}$ compound resulted in epitaxial matching between the crystallites with either $a\perp$ or $c\perp$. This resulted in films that were mainly $a\perp$ with b, c twinning. Occasionally, however, $a\perp$ material was found epitaxially oriented on the substrate

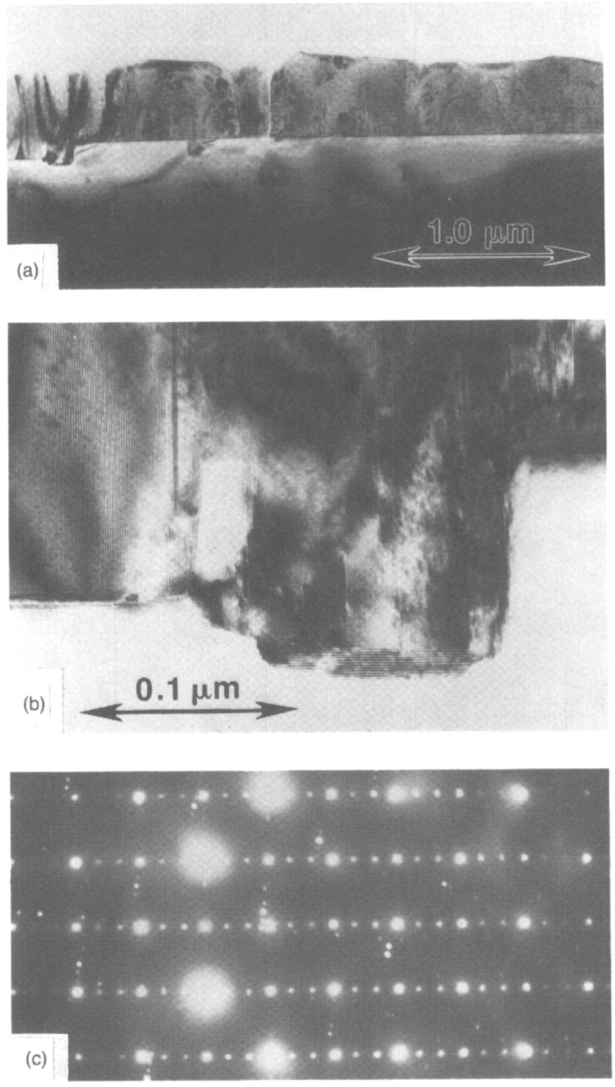

FIG. 8. TEM cross-sectional view of a 0.3 μm $Ho_1Ba_2Cu_3O_{7-x}$ film on a $SrTiO_3$ substrate. A low-magnification view (a) shows the surface morphology of the annealed films along with cracks which extended into the substrate. A higher magnification of the left side of (a) is given in (b) which shows two orientations of the ~11.7 Å lattice fringes perpendicular to the c axis of the 1:2:3 material corresponding to the $a\perp$ and $c\perp$ material. A selected area diffraction pattern (c) incorporating both substrate and film shows the epitaxial alignment with the substrate.

[vertical fringes in Fig. 8(b)]. Selected area diffraction patterns of the substrate and film (~1 μm spot size) confirmed the epitaxial alignment of the 1:2:3 material with the $SrTiO_3$ [as shown in Fig. 8(c)]. Almost all of the material investigated with the TEM was crystalline and epitaxially aligned [the fringeless region of Fig. 8(b) was oriented with the c-axis normal to the micrograph]. The interface between substrate and film appeared clean and sharp, with no amorphous boundary layer or evidence of structural relaxation associated

with interdiffusion. No precipitates were noted in the films. Occasional, randomly oriented microcrystallites were noted in some areas, probably resulting in the small component of randomly oriented polycrystalline material found in the x-ray data.

Plane-view SEM micrographs of the annealed superconducting films showed that their surface morphology had changed radically during annealing due to crystallization into *b*, *c* twins and cracking, the latter probably due to an a thermal expansion mismatch between the film and (100) $SrTiO_3$ substrate. The *b*, *c* twinning implied by the TEM and x-ray data became obvious at the edges of some of the films (as in Fig. 9) where the annealed $a\perp$ material did not form a continuous film. Long platelets, with the *b* axis oriented in the long direction and the *c* axis in the narrow dimension, formed a cross-hatched lattice due to *b*, *c* twinning. The relief of Fig. 9 suggests that the growth rate along the *a* axis (out of the figure) may be larger than in the *c*-axis direction for these films.

The resistive transition widths of our films should be sharpened considerably by optimizing the annealing conditions. Film contamination is known to occur during the annealing process by interdiffusion with the substrate, accompanied by intermediate phase formation. This lowers T_c and broadens the transition width, ΔT_c. Lower substrate temperatures during deposition and shorter times spent at high temperatures during the annealing process should mitigate these effects.

A lack of oxygen stoichiometry throughout the film would also explain the ~ 10 K superconducting transition widths. Both T_c and ΔT_c depend strongly on local oxygen stoichiometry, x, for $Ho_1Ba_2Cu_3O_{7-x}$ (Ref. 37). The measured lattice constants ($a\perp$, $a = 3.84 \pm 0.005$ Å and $c\perp$, $c = 11.65 \pm 0.01$ Å) deviate significantly from the measured $a = 3.82$ Å and $c = 11.66$ Å of fully oxygenated ($x = 0$) $Ho_1Ba_2Cu_3O_{7-x}$ bulk material.[38] To explain the large $a = 3.84$A would require either $0.3 < x < 0.55$ (yielding $T_c = 55$ K material) or oxygenated material that is strained by the constraint of lattice-matching to the substrate. Since $T_c > 80$ K for these films, the most reasonable explanation would involve an oxygen stoichiometry $x < 0.1$ that is determined by the strains imposed by epitaxy with the substrate.

Although the high-temperature (~ 900 °C) anneal used for these films resulted in formation of the superconducting orthorhombic phase, the implications of these results and of bulk annealing studies is to move to lower temperature depositions and anneals to reduce thermal cracking and strains as well as to minimize interdiffusion and intermediate phase formation. Recent experiments have characterized the oxygen stoichiometry (and lattice constants) versus temperature of $Y_1Ba_2Cu_3O_{7-x}$ for a range of oxygen pressures during the anneal.[39] The highest T_c's correspond to the maximally distorted (highest equilibrium oxygen content) orthorhombic phase following annealing. This implies that by adjusting the oxygen pressure and temperature during deposition to be in equilibrium with the high-T_c orthorhombic phase, superconducting as-deposited films with smoother morphology can be made at much

FIG. 9. SEM plane view of a selected region of an annealed 1 μm $Ho_1Ba_2Cu_3O_{7-x}$ film on $SrTiO_3$. The *b*, *c* twinning of the superconductor as well as the preferential growth along the *a* axis (out of the figure) is seen in this thin region. The *c* axis is in the plane of the micrograph across the narrow dimension of the flat platelets.

lower temperatures. Indeed, recent work by Venkatesan, *et al.*,[40] reports low-temperature (600 °C) formation of orthorhombic $Y_1Ba_2Cu_3O_{7-x}$ films on ZrO_2-coated Si which superconduct at T_c ($R = 80$) = 80 K. The effects of interface reactions were greatly reduced but the oxygen pressure (5 mTorr) was not optimized and (as in Fig. 6), the superconducting transitions were broadened.

IV. SUMMARY

In conclusion, the 248-nm pulsed-laser vaporization process for $Ho_1Ba_2Cu_3O_7$ and $Y_1Ba_2Cu_3O_7$ pellets shows two distinct regimes: evaporation and ablation. Evaporation dominates for energy densities between 0.11 and $\sim$0.5 J cm^{-2} and results in nonstoichiometric (holmium- or yttrium-deficient) thin films corresponding to low rare-earth metal or metal-oxide vapor pressure at high temperatures. For energy densities $>$0.6 J cm^{-2} a laser plasma is formed and stoichiometry is preserved in films deposited normal to the irradiated pellet. The laser-induced plasma fluorescence initiates and reaches a maximum within the laser pulse, exhibiting both atomic and molecular excited species which continue to be formed up to 1 μs later. The nature of the ablation process and of the interaction of the laser plasma with the pellet and ejected vapor is currently not understood in detail.

Microstructural analysis of the films shows highly epitaxially oriented films of mixed $a\perp$ and $c\perp$ orientations. The $c\perp$ orientation is preferred close to the substrate with the $a\perp$ orientation occupying $\sim$90% of the film volume. Highly textured films with preferential growth along the *a* axis and *b*, *c* twinning are formed under the high-temperature annealing conditions employed in this study. Evidence for oriented impurity phase(s) and a lack of oxygen stoichiometry in the films may explain the broad (10 K) superconducting transitions of these films.

Efforts to produce higher quality superconducting thin films by the pulsed laser deposition technique will require further characterization of the ablation and transport processes in order to produce films of uniform local stoichiometry and uniformly smooth morphology. Formation of the high-T_c orthorhombic phase at low temperature with maximal oxygenation will require careful correlation of deposition, annealing and substrate conditions with microstructural analysis of the films.

Note added in proof: Since this manuscript was submitted two relevant papers have been published, DeSantolo *et al.*[41] have used laser evaporation of a target composed of BaF_2, Y_2O_3, and CuO and annealed in wet oxygen to produce $Y_1Ba_2Cu_3O_{7-x}$ films with high critical current densities. Also, Auciello *et al.*[42] have performed a spectral survey of the XeCl (308 nm) laser-produced plasma from $Y_1Ba_2Cu_3O_{7-x}$ irradiated pellets and have found no molecular emission, in contrast to the molecular emission noted both in this paper and Ref. 35 using 248 nm irradiation.

ACKNOWLEDGMENTS

The authors gratefully acknowledge the excellent technical assistance of P. L. Hatmaker, H. E. Harmon, J. O. Ramey, P. H. Fleming and F. M. Rau. This work was sponsored by the Director's Research and Development fund at Oak Ridge National Laboratory and the Division of Materials Science, U.S. Department of Energy, under contract DE-AC05-840R21400 with Martin Marietta Energy Systems, Inc.

REFERENCES

[1]J. F. Ready, Appl. Phys. Lett. **3**, 11 (1963).
[2]J. F. Ready, *Effects of High Power Laser Radiation* (Academic, New York, 1971).
[3]H. Schwarz and H. A. Tourtellotte, J. Vac. Sci. Technol. **6**, 373 (1969).
[4]M. Hanabusa, M. Suzuki, and S. Nishigaki, Appl. Phys. Lett. **38**, 385 (1981).
[5]H. M. Smith and A. F. Turner, Appl. Opt. **4**, 147 (1965).
[6]P. D. Zavitsanos and W. E. Saver, J. Electrochem. Soc. **115**, 109 (1968).
[7]G. Hass and J. B. Ramsey, Appl. Opt. **8**, 1115 (1969).
[8]V. S. Ban and D. A. Kramer, J. Mater. Sci. **5**, 978 (1970).
[9]J. T. Cheung, Appl. Phys. Lett. **43**, 255 (1983).
[10]D. Lubben, S. A. Barnett, K. Suzuki, S. Gorbatkin, and J. E. Greene, J. Vac. Sci. Technol. B **3**, 986 (1985).
[11]D. Dimitrov, S. Metev, I. Gugov, and V. Kozhukharov, J. Mater. Sci. Lett. **1**, 334 (1982).
[12]H. Sankur, Mat. Res. Soc. Symp. Proc. **29**, 373 (1984).
[13]S. V. Gaponov, B. M. Luskin, B. A. Nesterov, and N. N. Salaschenko, Sov. Phys.-Solid State **19**, 1736 (1978).
[14]J. J. Dubowski, D. F. Williams, P. B. Sewell, and P. Norman, Appl. Phys. Lett. **46**, 1081 (1985).
[15]N. P. Ong, G. Kote, and J. T. Cheung, Phys. Rev. B **28**, 2289 (1983).
[16]S. V. Gaponov, B. M. Luskin, and N. N. Saloschenko, Solid State Commun. **39**, 301 (1981).
[17]D. Dijkamp, T. Venkatesan, X. D. Wu, S. A. Shaheen, N. Jisrawi, Y. H. Min-Lee, W. L. McLean, and M. Croft, Appl. Phys. Lett. **51**, 619 (1987).
[18]D. N. Mashburn, D. B. Geohegan, D. Eres, D. H. Lowndes, L. A. Boatner, B. C. Sales, S. J. Pennycook, R. J. Culbertson, E. Sonder, and D. K. Christen, Mat. Res. Soc. Symp. Proc. **99**, 699 (1988).
[19]L. Lynds, B. R. Weinberger, G. G. Peterson, H. A. Krasinski, Mater. Res. Soc. Symp. Proc. **99**, 707 (1988).
[20]H. S. Kwok, P. Mattocks, D. T. Shaw, L. Shi, X. W. Wang, S. Witanuchi, Q. Y. Ying, J. P. Sheng and P. Bush, Mat. Res. Soc. Symp. Proc. **99**, 735 (1988).
[21]K. Moorjani, J. Bohandy, F. J. Adrian, B. F. Kim, R. D. Shull, C. K. Chiang, L. J. Swartzendruber, and L. H. Bennett, Phys. Rev. B **36**, 4036 (1987).
[22]J. Narayan, N. Biunno, R. Singh, O. W. Holland, and O. Auciello, Appl. Phys. Lett. **51**, 1845 (1987).
[23]T. Venkatesan, X. D. Wu, A. Inam, and J. B. Wachtman, Appl. Phys. Lett. **52**, 1193 (1988).
[24]For a photograph of the irradiated pellet and the resulting plume see

MRS Bull. **XIII**, 3 (March 1988) cover photograph.
[25]P. K. Bhat, J. J. Dubowski, and D. F. Williams, Phys. Status Solidi A **96**, K9 (1986).
[26]P. E. Dyer, S. D. Jenkins, and J. Sidhu, Appl. Phys. Lett. **49**, 453 (1986).
[27]O. Auciello, A. R. Krauss, J. Santiago-Aviles, A. F. Schreiner, and D. M. Gruen, Appl. Phys. Lett. **52**, 239 (1988).
[28]A. Inam, X. D. Wu, T. Venkatesan, S. B. Ogale, C. C. Chang, and D. Dijkamp, Appl. Phys. Lett. **51**, 1112 (1987).
[29]G. V. Samsonov, Ed., *The Oxide Handbook* (IFI/Plenum, New York, 1982), 2nd ed.
[30]K. Tachikawa, I. Watanabe, S. Kosuge, and D. M. Ono, Mat. Res. Soc. Symp. Proc. **99**, 723 (1988).
[31]I. V. Nemchinov and S. P. Popov, JETP Lett. **11**, 312 (1970).
[32]G. A. Brost, C. L. Bohn, M. L. Crawford and B. W. Mullins, Mat. Res. Soc. Symp. Proc. **74**, 217 (1987).
[33]L. Lynds and B. A. Woody, Electron. Spectrosc. Relat. Phenom. **29**, 147 (1983).
[34]N. G. Utterback, S. P. Tang, and J. F. Friichteniicht, Phys. Fluids **19**, 900 (1976).
[35]S. G. Hansen and T. E. Robitaille, Appl. Phys. Lett. **50**, 359 (1987).
[36]T. Venketesan, X. D. Wu, A. Inam, and J. B. Wachtman, Appl. Phys. Lett. **52**, 1193 (1988).
[37]B. C. Sales, Y. C. Kim, J. R. Thompson, D. K. Christen, L. A. Boatner and S. T. Sekula, Mat. Res. Soc. Symp. Proc. **99**, 591 (1988).
[38]B. C. Sales (unpublished data).
[39]E. D. Specht, C. J. Sparks, A. G. Dhere, J. Brynestad, O. B. Cavin, and D. M. Kroeger, submitted to Phys. Rev. B.
[40]T. Venkatesan, E. W. Chase, X. D. Wu, A. Inam, C. C. Chang, and F. K. Shokoohi, submitted to Appl. Phys. Lett.
[41]A. M. DeSantolo, M. L. Mandich, S. Sunshine, B. A. Davidson, R. M. Fleming, P. Marsh, and T. Y. Kometani, Appl. Phys. Lett. **52**, 1995 (1988).
[42]O. Auciello, S. Athavale, O. E. Hankins, M. Sito, A.F. Schreiner, and N. Biunno, Appl. Phys. Lett. **53**, 72 (1988).